

## Supporting Information

### Achieving high thermoelectric conversion efficiency in $\text{Bi}_2\text{Te}_3$ -based stepwise legs through bandgap and chemical potential engineering

Rafal Knura,<sup>‡12</sup> Mykola Maksymuk,<sup>‡1</sup> Taras Parashchuk<sup>\*1</sup> and Krzysztof T. Wojciechowski<sup>\*1</sup>

<sup>1</sup>Thermoelectric Research Laboratory, Department of Inorganic Chemistry, Faculty of Materials Science and Ceramics, AGH University of Krakow, Mickiewicz Ave. 30, 30-059 Krakow, Poland

<sup>2</sup>Department of Science, Graduate School of Science and Technology, Kumamoto University, 2 Chome-39-1 Kurokami, Chuo Ward, 860-8555 Kumamoto, Japan

\*Corresponding authors: wojciech@agh.edu.pl; parashchuk@agh.edu.pl

‡ These authors contributed equally to this work.

#### 1. Experimental details

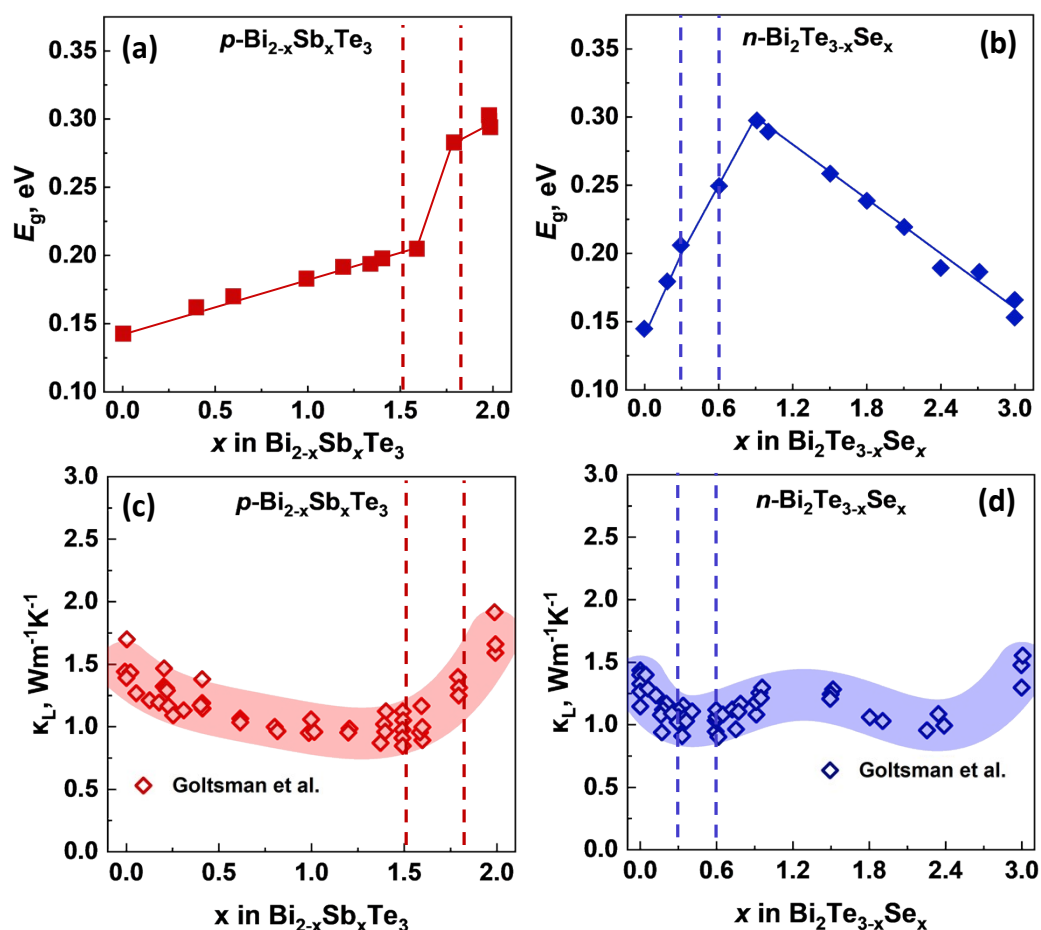


**Figure S1.** Bandgap (a, b) and lattice thermal conductivity (c, d) as a function of chemical composition  $x$  in  $n$ -type  $\text{Bi}_2\text{Te}_{3-x}\text{Se}_x$  (a, c) and  $p$ -type  $\text{Bi}_{2-x}\text{Sb}_x\text{Te}_3$  alloys (b, d). The images were made using data available in [1].

The measurement of the energy parameters of thermoelectric samples was performed using laboratory-testing equipment presented in Figure S2.

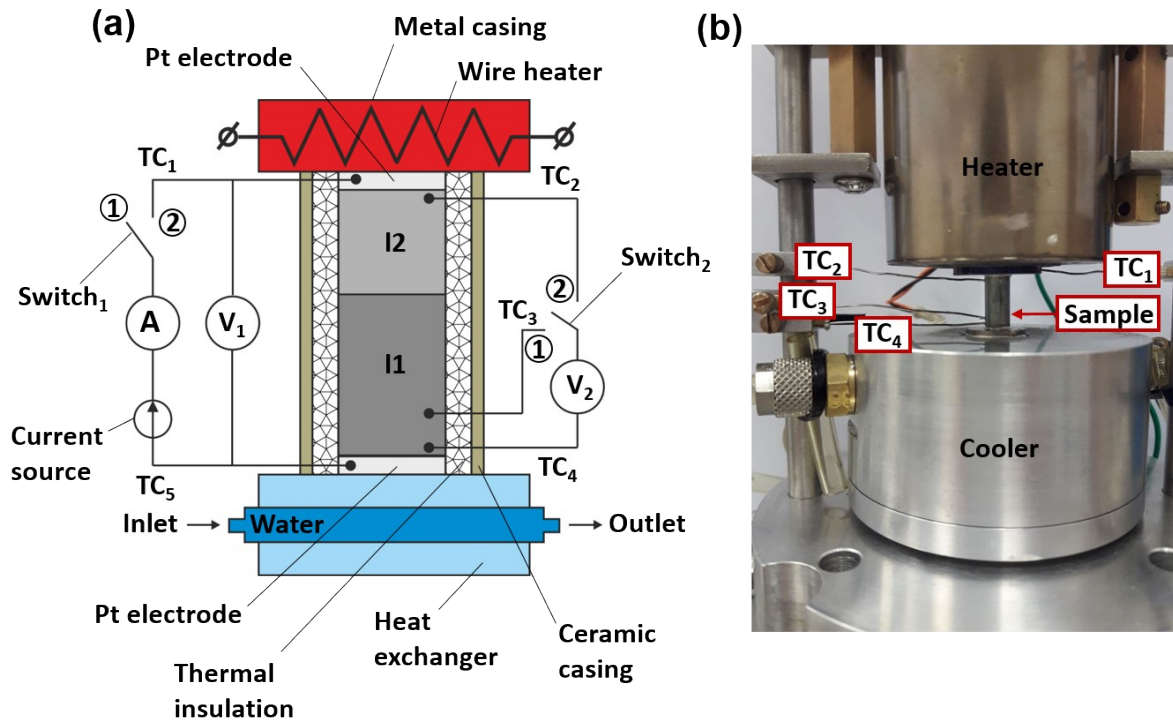


**Figure S2.** (a) Schematic view and (b) physical image of the apparatus for measurement of output energy parameters of thermoelectric legs.

The measuring instrument consists of the heating and cooling parts. The thermoelectric stepwise sample is placed between them. The heating of the hot sample side is performed by the wire heater which is implemented in the metal casing while the heat dissipation from the cold side of the stepwise sample is provided by the water flow through the channels of the heat exchanger. To improve the heat transfer between a pair of "heater/sample" and "sample/cooler", the measurement setup additionally includes the highly-conductive platinum (Pt) electrodes. To prevent heat losses from the side surfaces, the sample is placed in a thermal insulation layer which is fixed in the thick ceramic casing. To minimize the heat losses due to convection and radiation, the measurements of samples were carried out in a vacuum.

The measurement principle of the energy parameters of the stepwise sample can be seen in Figure S2a. Firstly, switch<sub>1</sub> and switch<sub>2</sub> were set in position ① where the achieved temperature difference applied to the sample sides was recorded by the thermocouples TC<sub>1</sub> and TC<sub>5</sub> placed in the Pt-electrodes, and the generated open-circuit voltage of the whole sample was measured using the V<sub>1</sub>-voltmeter. Then, the measurement of the  $OCV_1$  value of the lower I1-layer is performed with the

help of the  $V_2$ -voltmeter and the thermocouples  $TC_3$  and  $TC_4$ . These data were used for the determination of the Fourier heat  $Q_F$  which flowed across the sample according to the Eq. (S1):

$$Q_F = \frac{OCV_1}{S_1(\bar{T})} \times \frac{A}{l} \times \kappa_1(\bar{T}) \quad (S1)$$

where  $OCV_1$  is the open-circuit voltage generated by the lower thermoelectric layer;  $l$  and  $A$  are the distance between measurement points ( $\sim 1.5$  mm) and the cross-sectional area of the sample, respectively;  $S_1(\bar{T})$  and  $\kappa_1(\bar{T})$  are the Seebeck coefficient and thermal conductivity of the thermoelectric material of the lower thermoelectric layer at temperature  $\bar{T}$ , which is the average value of the temperatures measured by the thermocouples  $TC_3$  and  $TC_4$ .

Finally,  $switch_1$  and  $switch_2$  were set in position ②, where the current source delivered the electric current which flowed through the sample. In this case, the measurement of the electric voltage of the stepwise sample was carried out using the  $V_2$  voltmeter and the thermocouples  $TC_2$  and  $TC_4$  which were placed in the lower and higher layers  $l_1$  and  $l_2$ , respectively. The input electric current was established with the value, which produces half of the open-circuit voltage generated by the sample. In this case, the maximum electric power can be achieved. The obtained experimental data was used for the determination of the internal sample resistance  $R$ :

$$R = \frac{U}{I} \times \frac{L}{d} \quad (S2)$$

where  $U$  is the output electric voltage of the sample;  $I$  the electric current which flows through the sample measured by A-amperemeter;  $L$  is the total length of the sample and  $d$  is the distance between the measurement points.

The output electric power  $P_{out}$ , input heat power  $Q_{in}$  and efficiency  $\eta$  of the thermoelectric stepwise sample were calculated using the following equations [2]:

$$P_{out} = \frac{OCV^2}{4R}, \quad (S3)$$

$$Q_{in} = (IT_h S_2(T_h) + Q_F - \frac{1}{2} I^2 R), \quad (S4)$$

$$\eta = \frac{P_{out}}{Q_{in}}, \quad (S5)$$

where  $OCV$  is the open-circuit voltage of the sample;  $T_h$  is the temperature of the hot side of the sample;  $S_2(T_h)$  is the Seebeck coefficient of the high-temperature thermoelectric layer at temperature  $T_h$ . During the calculation, the Thompson heat was assumed to be equal to 0.

## 2. Finite element analysis

Analytical expression for calculation of the optimal layer height [3]:

$$h_{12} = h \frac{\bar{\kappa}_{12}(T_h - T_s)}{\kappa_{ef}(T_h - T_c)} \cdot \left[ 1 + \frac{T_h - T_c}{T_h + T_c} \cdot \frac{\sqrt{1 + (ZT)_{ave}^{12}} - 1}{\sqrt{1 + (ZT)_{ave}^{12}} + 1} \cdot \frac{\bar{\kappa}_{11}(T_s - T_c)}{\kappa_{ef}(T_h - T_c)} \right], \quad (S6)$$

$$h_{11} = h - h_{12}, \quad (S7)$$

where  $h_{11}$  and  $h_{12}$  are the heights of the first and second layer, respectively;  $h$  is the total height of the stepwise leg;  $T_s$  is the intersection temperature on the contact boundary of both layers which is defined from the temperature dependence of the figure of merit of the used thermoelectric materials

(Figure 7d);  $(ZT)_{ave}^{12} = \frac{1}{T_h - T_s} \int_{T_s}^{T_h} (ZT)_{12} dT$  is the average figure of merit of the thermoelectric material

for the second layer;  $\bar{\kappa}_{11}, \bar{\kappa}_{12}$  are the average thermal conductivity of the first and second layer,

respectively, which were defined as  $\bar{\kappa}_{11} = \frac{1}{T_s - T_c} \int_{T_c}^{T_s} \kappa_{11}(T) dT$ ,  $\bar{\kappa}_{12} = \frac{1}{T_h - T_s} \int_{T_s}^{T_h} \kappa_{12}(T) dT$ ;

$\kappa_{ef} = \frac{\bar{\kappa}_{11}(T_s - T_c) + \bar{\kappa}_{12}(T_h - T_s)}{T_h - T_c}$  is the effective thermal conductivity of the stepwise leg.

**Table S1.** Input parameters for numerical simulation

Parameter	Value	
	$n\text{-Bi}_2\text{Te}_{3-x-y}\text{Se}_x\text{Cl}_y$ leg	$p\text{-Bi}_{2-x}\text{Sb}_x\text{Te}_3$ leg
<b>Geometry</b>		
The cross-section area, $A$	28.26 mm <sup>2</sup>	
The height of the first layer, $h_{11}$	8 mm	6 mm
The height of the second layer, $h_{12}$	4 mm	6mm
The total height, $h$	12 mm	
<b>Materials</b>		
The first layer, $l_1$	$x = 0.6, y = 0.015$	$x = 1.8$
The second layer, $l_2$	$x = 0.3, y = 0.03$	$x = 1.52$

Temperature conditions	
The temperature of the hot side, $T_h$	350-675 K
The temperature of the cold side, $T_c$	300 K

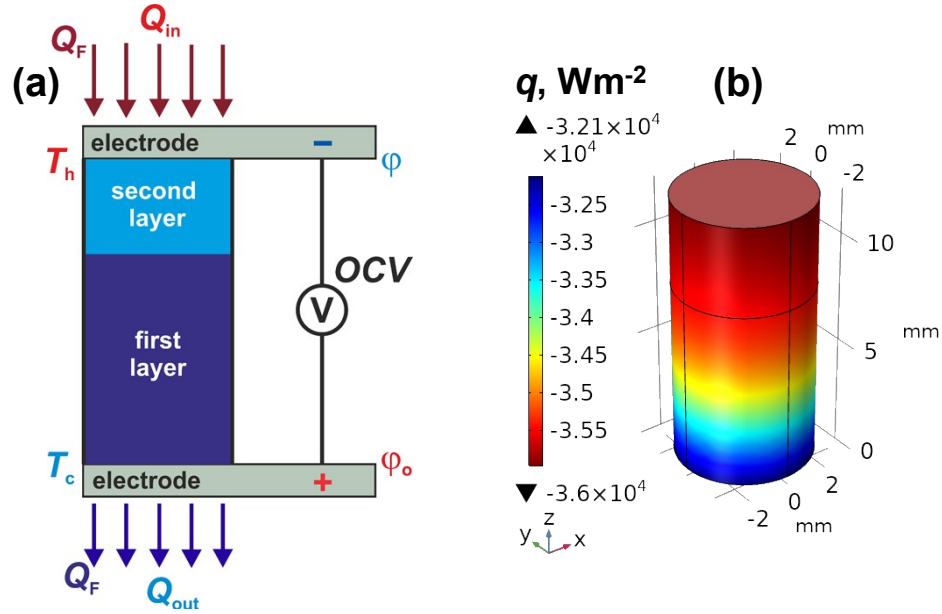


**Figure S3.** Physical model for open-circuit voltage mode modeling by FEM (a) and distributions of the heat flux density (b) in the  $n$ -type stepwise thermoelectric leg.

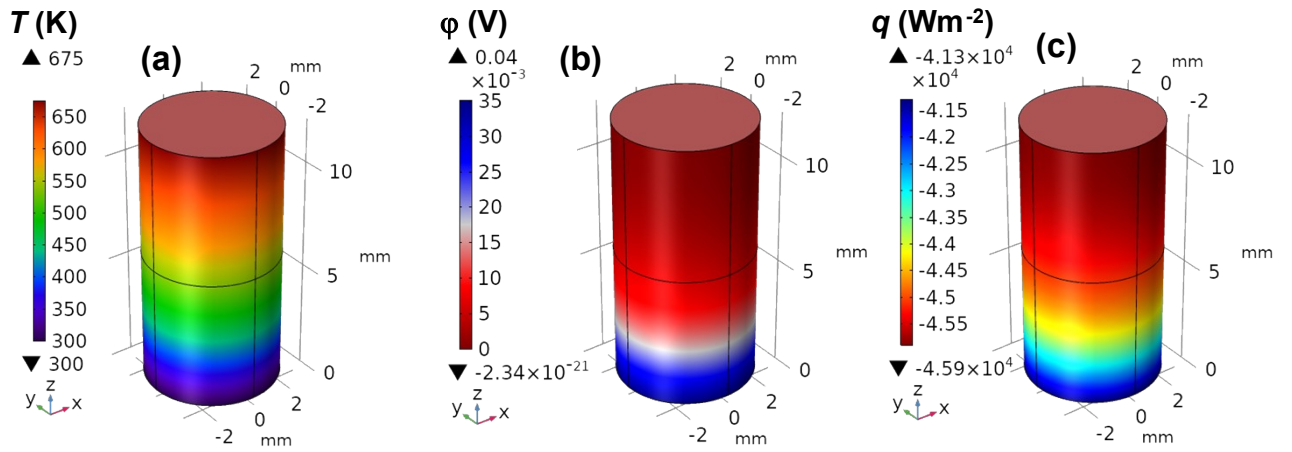


**Figure S4.** The distributions of temperature (a), electric potential (b), and heat flux density (c) in the  $p$ -type stepwise thermoelectric leg.

Analytical expressions for energy parameters determination [3]:

$$OCV = \int_{T_c}^{T_s} S_{11}(T)dT + \int_{T_s}^{T_h} S_{12}(T)dT, \quad (S8)$$

$$R = \frac{1}{A} \left( \frac{h_{l1}}{T_s - T_c} \cdot \int_{T_c}^{T_s} \frac{1}{\sigma_{l1}(T)} dT + \frac{h_{l2}}{T_h - T_s} \cdot \int_{T_s}^{T_h} \frac{1}{\sigma_{l2}(T)} dT \right), \quad (S9)$$

$$Q_{in} = \int_0^{2\pi} d\theta \int_0^r q|_{z=h} r dr, \quad (S10)$$

$$P_{out} = \frac{OCV^2}{4R}, \quad (S11)$$

$$\eta = \frac{P_{out}}{Q_{in}}, \quad (S12)$$

where the subscript indices “1” and “2” denote the first and second leg layers, respectively,  $A$  is the cross-section area of the sample, and the intersection temperature  $T_s$  is defined due to the temperature distribution along the height of the thermoelectric leg.

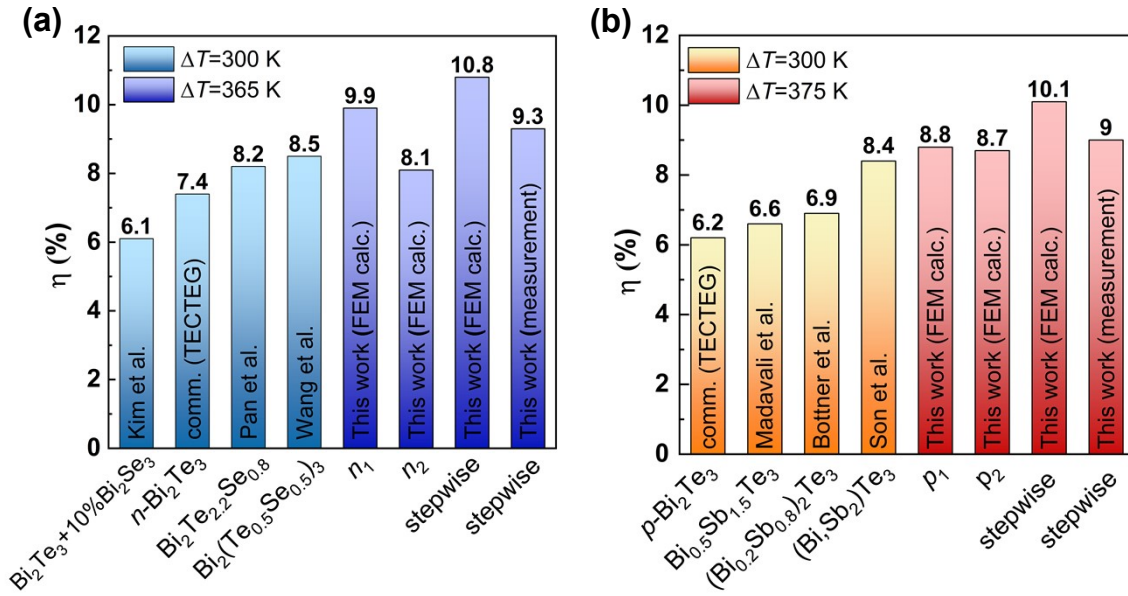


**Figure S5.** Energy conversion efficiency of (a)  $n$ - and (b)  $p$ -type stepwise legs compared with the estimated performance of the thermoelectric  $\text{Bi}_2\text{Te}_3$ -based unilegs reported in [4-10].

## References

1. Goltsman BM, Kudinov VA, Smirnov IA. Thermoelectric Semiconductor Materials Based on  $\text{Bi}_2\text{Te}_3$ . Moscow: Nauka; 1972 [in Russian]
2. A.S. Okhotin, A.A. Yefremov, V.S. Okhotin, and A.S. Pushkarskiy, Thermoelectric Generators. U.S. Army Foreign Science and Technology Center, 1972.

3. M. Maksymuk, T. Parashchuk, A. Burbelko, K. T. Wojciechowski, Thermoelectric converter with stepwise legs for high energy conversion efficiency, *Chem. Eng. J.* 472 (2023) 144899 <https://doi.org/10.1016/J.CEJ.2023.144899>
4. Kim H, Han MK, Yo CH, Lee W, Kim SJ. Effect of Bi<sub>2</sub>Se<sub>3</sub> Nanoparticle Inclusions on the Microstructure and Thermoelectric Properties of Bi<sub>2</sub>Te<sub>3</sub>-Based Nanocomposites, *J Electron Mater* 2012;41:3411–3416. <https://doi.org/10.1007/s11664-012-2255-7>
5. <https://thermoelectric-generator.com/wp-content/uploads/2014/07/Ingot-Raw-Material-BiTe-N-and-P.pdf>
6. Y. Pan, T.R. Wei, C.F. Wu, J.F. Li, Electrical and thermal transport properties of spark plasma sintered *n*-type Bi<sub>2</sub>Te<sub>3-x</sub>Se<sub>x</sub> alloys: the combined effect of point defect and Se content, *J. Mater. Chem. C* 3 (2015) 10583–10589. <https://doi.org/10.1039/C5TC02219C>
7. S. Wang, G. Tan, W. Xie, G. Zheng, H. Li, J. Yang, X. Tang, Enhanced thermoelectric properties of Bi<sub>2</sub>(Te<sub>1-x</sub>Se<sub>x</sub>)<sub>3</sub>-based compounds as *n*-type legs for low-temperature power generation, *J. Mater. Chem.* 22 (2012) 20943–20951. <https://doi.org/10.1039/C2JM34608G>
8. B. Madavali, S.J. Hong, Enhanced Thermoelectric Properties of *p*-type Bi<sub>0.5</sub>Sb<sub>1.5</sub>Te<sub>3</sub> Thermoelectric Materials by Mechanical Alloying and Spark Plasma Sintering, *J. Electron. Mater.* 45 (2016) 6059–6066. <https://doi.org/10.1007/s11664-016-5011-6>
9. H. Böttner, D.G. Ebling, A. Jacquot, U. Kühn, J. Schmidt, Melt spinning preparation of Bismuth Telluride and partially alloying with IV-VI compounds for thermoelectric application, in: *Proc 26th Int. Conf. Thermoelectr.*, Jeju Island, Korea, 2007: p. 1044. <https://doi.org/10.1557/PROC-1044-U04-01>
10. J.H. Son, M.W. Oh, B.S. Kim, S.D. Park, B.K. Min, M.H. Kim, H.W. Lee, Effect of ball milling time on the thermoelectric properties of *p*-type (Bi,Sb)<sub>2</sub>Te<sub>3</sub>, *J. Alloys Compd.* 566 (2013) 168–174. <https://doi.org/10.1016/j.jallcom.2013.03.062>